Charge transport and recombination in P3HT:PbS solar cells

Yuliar Firdaus,[1] Erwin Vandenplas,[2] Adis Khetubol,[1] David Cheyns,[2] Robert Gehlhaar,[2] and Mark Van der Auweraer [1,a)]

[1] *Laboratory of Photochemistry and Spectroscopy, Division of Molecular Imaging and Photonics, Chemistry Department, KULeuven, Celestijnenlaan 200F, B2404, 3001 Leuven, Belgium*

[2] *Imec vzw, Kapeldreef 75, B-3001 Leuven, Belgium*

The charge carrier transport in thin film hybrid solar cells is analyzed and correlated with device performance and the mechanisms responsible for recombination loss. The hybrid bulk heterojunction consisted of a blend of poly(3-hexylthiophene) (P3HT) and small size (2.4 nm) PbS quantum dots (QDs). The charge transport in the P3HT:PbS blends was determined by measuring the space-charge limited current in hole-only and electron-only devices. When the loading of PbS QDs exceeds the percolation threshold a significant increase of the electron mobility is observed in the blend with PbS QDs. The hole mobility, on the other hand, only slightly decreased upon increasing the loading of PbS QDs. We also showed that the photocurrent is limited by the low shunt resistance rather than by space-charge effects. The significant reduction of the fill factor at high light intensity suggests that under these conditions the non-geminate recombination dominates. However, at open-circuit conditions, the trap-assisted recombination dominates over non-geminate recombination.

a) mark.vanderauweraer@chem.kuleuven.be; phone 3216327496; fax 3216327990

I. INTRODUCTION

Colloidal quantum dots (QDs) of inorganic semiconductors are considered as viable potential substitutes for fullerene acceptors in photovoltaic devices. Low-bandgap lead-chalcogenide QDs such as PbS were shown to be a promising electron acceptor in hybrid bulk heterojunction (BHJ) solar cells due to their high electron mobility[1], broad and tunable absorption extending into the infrared[2] and the possibility for carrier multiplication[3–5]. Recently, the combination of narrow band-gap conjugated polymers (with more suitable energy levels and a better coverage of the solar spectrum) and a better passivation of the PbS surface led to a dramatic increase of the power conversion efficiency (PCE) of polymer:PbS QDs hybrid solar cells which reached up to 4.23%.[2,6–8]

We have demonstrated that the use of small (2.4 nm) quantum dots (QDs) and post deposition ligand exchange to 1,4-benzenedithiol (BDT) improves the PCE of poly(3-hexylthiophene) (P3HT):PbS hybrid solar cells up to 1%.[9] Further optimization of the architecture of the solar cell increased the average PCE further to 1.8%.[10] It was also shown that the ligand exchange of the original oleic acid (OLA) ligands to BDT clearly led to a more efficient photo-induced charge transfer in the P3HT:PbS system.[10] The electron transfer from P3HT to PbS QDs takes place on a time scale from tens of femtoseconds (fs) to a few nanoseconds (ns) which can be related to the occurrence of phase separation between donor and acceptor materials on a nanometer scale.[10]

For all solar cells, charge recombination competes with charge-extraction. The recombination of photogenerated charge carriers in polymer BHJ solar cells, which was attributed to several mechanisms, reduces the FF and the short-circuit current (J_{SC})[11]. In poly(3-hexylthiophene):[6,6]-phenyl C61 butyric acid methyl ester (P3HT:$PC_{60}BM$) solar cells, for example, geminate (monomolecular)[12,13], non-geminate (bimolecular)[14–16] or a combination of the two[11] recombinations has been proposed. Geminate recombination involves the recombination of a hole and an electron that originate from the same donor (or acceptor) excitation while for non-geminate recombination the hole and electron originate from absorption of two different photons. Trap-assisted recombination is usually neglected, except for organic solar cells (OSCs) with fast grown active-layers[17], OSCs with non-fullerene acceptors[18], or donors with limited short-range order[19]. Trap-assisted recombination involves trapping of one type of carrier at defect states within a donor or acceptor phase and its subsequent recombination with a free carrier in the other phase. The recombination in polymer:CdSe QDs film has been attributed to the presence of traps which are probably located on the QD surface.[6,20] The presence of trap states, which can also be partly responsible for a lower

carrier mobility, has been shown in cross-linked PbS film.[21] The efficient collection of photo-generated charge carriers at the electrodes, avoiding recombination, is a challenge which requires that the electrons and holes have separate continuous pathways to the electrodes without the need of passing through the material transporting the oppositely charged carrier. Furthermore, the transport of charge carriers towards the electrodes will be impeded by space-charge effects which were reported to limit the fill-factor (FF) and the efficiency of solar cells.[22–25] In order to avoid this space-charge effect, a proper balance of the mobilities of electrons and holes in respectively the acceptor material and the conjugated donor polymer, is required.[26,27]

In this paper, we present an investigation of the transport of electrons and holes in P3HT and PbS QDs blend photovoltaic device using the space-charge limited current (SCLC) method. Furthermore, the characterization of the electric-optical behavior allowed us to elucidate in a qualitative way the charge recombination mechanism in P3HT:PbS solar cells.

II. EXPERIMENTAL

A. Materials

The regioregular (RR)-P3HT (Sepiolid P200, RR:>96%; Mn: 13.9 kg/mol; PDI:1.71) was obtained from Rieke Metals. The poly(3,4-ethylenedioxythiophene):poly(styrene sulfonate) (PEDOT:PSS) (Clevios P VPAI 4083) used in this work was obtained from Heraeus. The colloidal PbS QDs with a core diameter of approximately 2.4 nm and capped by oleic acid (OLA) were purchased from Evident Technologies (Troy, NY). MoO_3 was obtained from Sigma Aldrich and used as purchased. The diodes were fabricated on pre-patterned and cleaned indium tin oxide (ITO) coated glass substrates (sheet resistance <20 Ω/□). The substrates were cleaned in milli-Q water, acetone and isopropanol, in an ultrasonic bath before treated in an ultraviolet-ozone chamber for 30 minutes.

B. Dielectric constant estimation.

The dielectric constant of the blended films was estimated by measuring the capacitance and the thickness of the films placed between two parallel electrodes. To estimate the capacitance, the films were connected in an RC circuit in series with a resistor (100 Ω), a signal generator (100 kHz) and a LeCroy 9400A digital oscilloscope. A Dektak surface profiler was used to measure the thickness of P3HT and P3HT:PbS blended films. The dielectric constant was then estimated according to the

parallel plate capacitance equation: $\varepsilon_r = \frac{Cd}{\varepsilon_0 A}$, where ε_r is the dielectric constant of the film, C is the capacitance, ε_0 is the permittivity of vacuum, A is the area of the electrodes and d is the film thickness.

C. Characterization of P3HT:PbS morphology.

The morphology of the active layers of the photovoltaic devices was determined with a Zeiss EM 902A transmission electron microscope (TEM). The films for the TEM measurements were formed by spin coating of the blend solutions (total concentration 7.6-12 mg/ml) onto a glass substrate covered by PEDOT:PSS. The spin-coated films were rinsed with water to lift-off the films from the glass substrate, and were then transferred to copper grids for testing.

D. Deposition of the active layer and ligand exchange in films containing PbS QDs.

First, a thin layer (~30 nm) of PEDOT:PSS was spin-coated at 3500 rpm for 60 s onto the ITO glass in air and then baked at 150°C for 15 minutes inside a glovebox. The PbS QDs or the blends of P3HT:PbS QDs (60, 75 and 90% loading of QDs) [9,10] were dissolved in chloroform at a concentration of 20-38 mg/ml (sum of the weight of the PbS core and P3HT). The loading by the QDs corresponds to the weight of PbS divided by sum of the weight of PbS and P3HT as these parameters could be determined unambiguously from the preparation of the solution. The actual weight and volume fraction of PbS in the film will be significantly smaller as also the mass and volume of the ligands have to be considered (see supporting information, SI [28]). P3HT was mixed with the solution of OLA-capped QDs for at least 1 hour at 70°C in a closed vial. Then the temperature was decreased and kept at 40° C for 15 minutes. This solution was spin-coated (1000 rpm for 60 s) in a nitrogen-filled glovebox on the PEDOT-PSS layer. The post-deposition ligand exchange to BDT was then carried out by soaking the film of neat PbS-OLA QDs or the blended film of P3HT:PbS-OLA in a 0.02 M solution of BDT in acetonitrile for 60 s followed by spinning the substrate at 1000 rpm for 30 s to remove the solvent and any residual BDT. All films were subsequently annealed at 150°C for 10 minutes inside a nitrogen-filled glove box.

E. Device fabrication and characterization.

The SCLC hole-only devices were fabricated using the following architectures: Glass/ITO/PEDOT:PSS/active-layer/MoO_3/Ag. First, a thin layer (~30 nm) of PEDOT:PSS was spin-coated at 3500 rpm for 60 s onto the ITO glass in air and

then baked at 150°C for 15 minutes inside a glovebox. After deposition of the active layer and ligand exchange (as described in section II C) on the PEDOT:PSS coated substrates, MoO_3 (10 nm) followed by Ag (100 nm) were deposited via thermal evaporation in a vacuum chamber at a base pressure of 1×10^{-7} mbar. The rate of evaporation of MoO_3 was maintained at 1 Å/s while the deposition rate of Ag was maintained at 6 Å/s.

The SCLC electron-only devices were fabricated using the following architecture: glass/ITO/ZnO/active-layer/Ca/Ag. Zinc acetate dihydrate (200 mg), 2-methoxyethanol (2 mL), and ethanolamine (55 μL) were mixed and stirred vigorously for 2 h at 60 °C in air.[29] This precursor solution was spin coated at 2000 rpm on to the cleaned ITO substrates to get a smooth ZnO film. Crystalline ZnO films were obtained by subsequent annealing of the sample at 250 °C for 30 min in air. After deposition of the active layer on top of the ZnO layer and ligand exchange, calcium (20 nm)/ Ag (100 nm) were deposited via thermal evaporation in a vacuum chamber at a base pressure of 1×10^{-7} mbar. The rate of evaporation of Ca was maintained at 1 Å/s while that of Ag was maintained at 6 Å/s. The final thickness of active-layer was measured using a Dektak D150 surface profilometer. The solar cells were fabricated using the following architecture: glass/ITO/PEDOT:PSS/active-layer/Ca/Ag.

The electrical characterization of hole-only and electron-only devices was performed inside the glovebox using a four-point probe configuration (see Fig. S1 [28]). The four-point probe measurements were used to avoid the necessity to correct the applied voltage for the effect of ITO, contact and cables resistance. The electrical characterization was performed using a Keithley 2602 “Source Meter” unit and an Agilent 4156C “Parameter Analyzer”.

The electrical characterization of the solar cell was performed inside the glovebox using the same four point configuration under illumination by a 1000W Xe arc lamp equipped with filters to simulate the AM 1.5 D spectrum (L.O.T. Oriel Solar Simulator). The lamp was calibrated using a bandpass filter (KG5, L.O.T. oriel) and a silicon detector. The incident light power was varied with neutral density filters.

III. RESULTS AND DISCUSSION

We attempted to study the charge carrier transport in P3HT:PbS photoactive layers using the space charge limited current (SCLC) approach. The single carrier device used in this approach allows the measurement of charge transport in a geometry and conditions very similar to those in hybrid solar cells (HSC). *E.g.* at a field in the range of $3x10^4$ to $5x10^4$ V/cm over the active layer the electron and hole densities in an operating HSC are respectively estimated at $6.5x10^{15}$ cm^{-3} and

$4.0x10^{14}$ cm^{-3} (calculation supporting information, SI [28]), which is comparable to those in a TOF experiment ($2.8x10^{14}$ cm^{-3}) [30] (calculation supporting information, SI [28]) and about one order of magnitude smaller than those obtained in hole only and electron only devices are (respectively $3.3x10^{16}$ cm^{-3} and $1.6x10^{16}$ cm^{-3}, calculation supporting information, SI [28]). In a FET configuration charge carrier densities of 10^{20} to 10^{24} cm^{-3} are present which can lead to significantly larger carrier mobilities.[31–33] Assuming Ohmic contacts for the injection and extraction of the charge carriers and a trap-free transport, the current density, J_{SCL}, is given by the Mott-Gurney's equation[34]

$$J_{SCL} = \left(\tfrac{9}{8}\right)\varepsilon_r\varepsilon_0\mu\left(\left(V - V_{bi}\right)^2 / L^3\right) \quad (1)$$

where ε_0 is the permittivity of free space, ε_r the static dielectric constant of the active layer, V the applied voltage, V_{bi} the built in potential difference, L the thickness of the films and μ the charge carrier mobility.

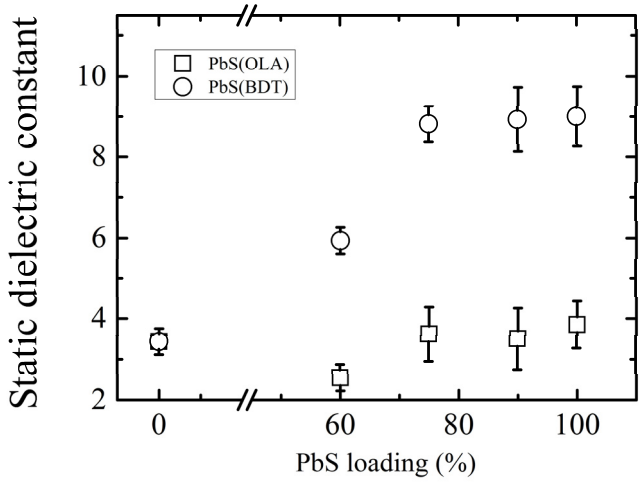

FIG. 1. Effective dielectric constant of P3HT:PbS blended films for different PbS loading and of a film of neat PbS QDs before (PbS-OLA) and after BDT treatment. The values were derived from the capacity of a film incorporated in a parallel plate capacitor.

In order to estimate the charge carrier mobility using Mott-Gurney's equation (eq.1), it is necessary to know the effective dielectric constant of the active layer of the single carrier device. The static dielectric constant was measured by the determination of the capacity of a parallel plate capacitor where the film was used as dielectric (see experimental details). As shown in Fig. 1, the static dielectric constant of P3HT measured with this method is around 3.4. This is in agreement with the dielectric constant of P3HT found in the literature.[35–37] Furthermore, while the dielectric constant increases only slightly upon

the addition of PbS-OLA QDs to the P3HT matrix (see Fig. 1) it is increased significantly after the blended films are treated with BDT. After BDT treatment a neat film of PbS QDs shows a much larger value for the dielectric constant (around 9) which is however smaller than the earlier reported value of around 18.[38]

For a two-component film it is also possible to estimate the dielectric constant using the Maxwell-Garnett effective medium theory[38]

$$\varepsilon = \varepsilon_m \frac{\varepsilon_i (1+2\delta) - \varepsilon_m (2\delta - 2)}{\varepsilon_m (2+\delta) + \varepsilon_i (1-\delta)} \quad (2)$$

where ε, ε_m, ε_i are dielectric constant of the film, the matrix (polymer and/or ligands), and the embedded PbS QDs respectively, and δ is the volume fraction of the embedded PbS QDs; the dielectric constant of the PbS QD blended films depends on the volume fraction of PbS in the QD ligand assembly and therefore depends also on the size of PbS QDs and type of ligand used. For PbS QDs with a size of 2.4 nm, the effective dielectric constant of neat films of PbS-OLA and PbS-BDT QDs (in this case ε_m is the dielectric constant of the ligands and ε_i is that of the PbS QDs) was estimated using eq. 2 to be approximately 3.7 and 9.15 (see Table S1 [28]); using a value of 169 [38] for ε_i of PbS, and of 2.5 and 4 for ε_m (for respectively OLA and BDT [39,40]).

Considering a volume fraction of PbS in the ligand matrix amounting to 15% and 32% for OLA and BDT ligands, respectively, the calculated value is in close agreement with our experimentally measured value of 3.85 and 9 for neat films of the PbS QDs (with OLA and BDT ligands, respectively) shown in Fig. 1 and Table S1 [28]. Both the increased volume fraction of PbS and the larger dielectric constant of BDT compared to OLA can explain the significant increase of dielectric constant of neat PbS and P3HT:PbS blended films after BDT treatment. Note that, for the blended films, the dielectric constant of the matrix, ε_m, was calculated using the expression:

$$\varepsilon_m(P3HT + ligand) = \frac{v_{P3HT} \times \varepsilon_{P3HT} + v_{ligand} \times \varepsilon_{ligand}}{v_{P3HT} + v_{ligand}} \quad (3)$$

where v_{P3HT} and v_{ligand} correspond to the volume fraction of P3HT and of the ligands. In contrast to P3HT:PbS-OLA blended films, the calculated dielectric constants of P3HT:PbS-BDT blended films shown in Table S1 [28] are 13 to 30% lower than the ones obtained from the measurements. The morphology of P3HT:PbS films before (with OLA ligand) and after ligand

exchange to BDT obtained using TEM is shown in Fig. S3 [28]. The images were obtained in the bright field mode without energy filter which means that the variations in image brightness could reflect thickness variation. The images of the blend films containing PbS QDs with the initial OLA ligands, (images a-c), show some irregular bright structures which are possibly regions with a low concentration of quantum dots suggesting a tendency of the QDs to form aggregates in the film. Furthermore, the reduction of the volume of the film upon evaporation of the solvent can induce some cracks at nanometer length scale. The significant increase (see images d-f) of the bright regions combined with the appearance of darker regions which contain QDs in at a higher concentration after the treatment of the films with BDT suggest a further clustering of the QDs. The cross-linking nature and smaller volume of this ligand links the PbS QDs together forming denser structures. This will be compensated by a reduction of density of the QDs in other (bright) regions. The morphological changes observed upon ligand exchange suggest that the post-deposition ligand exchange with BDT is successful.

In order to obtain either a hole-only or an electron-only device the work function of the electrodes has to be adjusted in such way that one electrode should be able to inject charge carriers in the semiconductor without any limitation while the other electrode should not be able to inject carriers of opposite sign; furthermore the latter electrode should be able to collect the injected carriers without any barrier.[34] A typical hole-only device can be produced by sandwiching poly(3,4-ethylenedioxythiophene) poly(styrenesulfonate) (PEDOT:PSS) and P3HT between two high work function electrodes such as ITO and gold (Au) (work function ~4.8 eV and 5.1 eV, respectively).[41,42] This should lead for holes to the expected ohmic contact between the electrodes and P3HT and should yield a clear quadratic dependence of the current density on the voltage, indicating a SCL current.

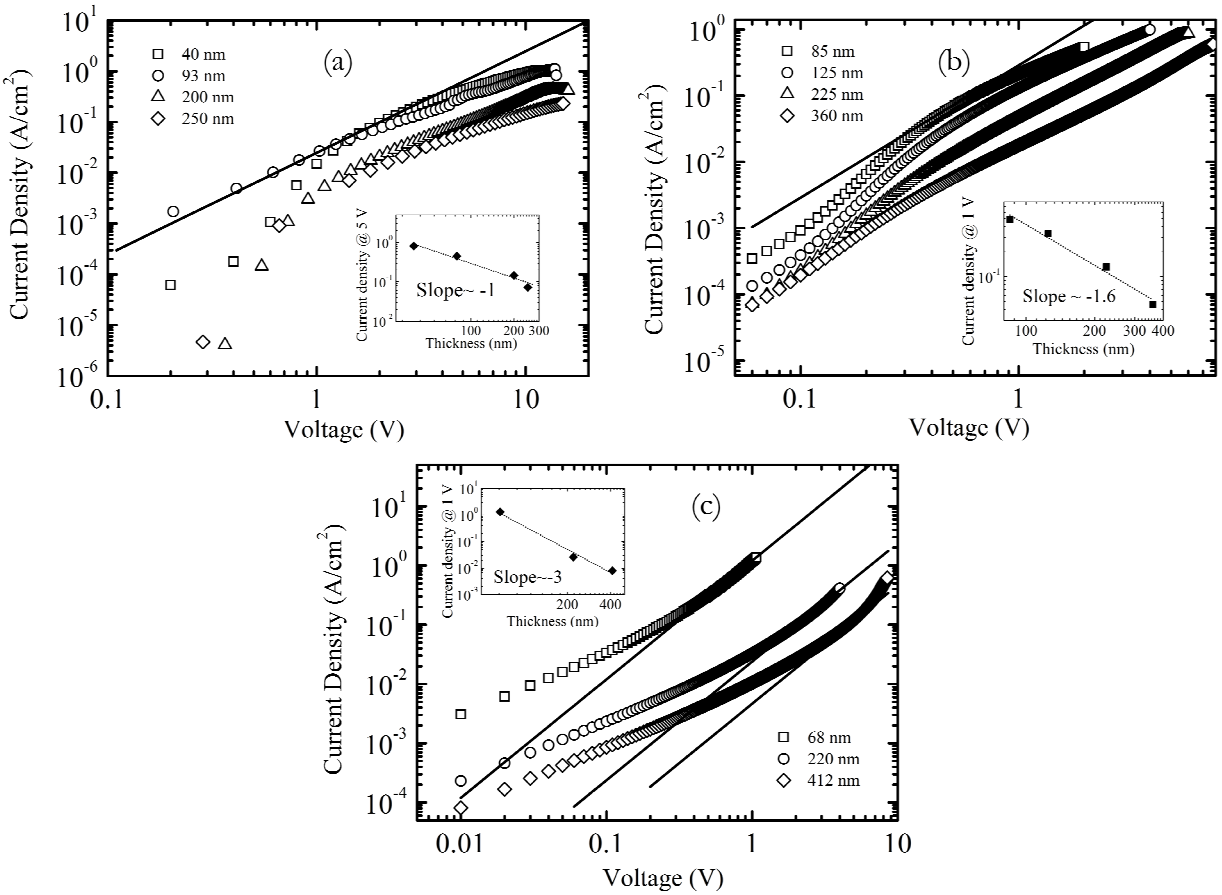

FIG. 2. Double logarithmic current density versus voltage (*J-V)* plots of hole-only devices of a film of neat regioregular-P3HT for different thicknesses and with a positive voltage applied to the ITO/PEDOT:PSS electrode. The solid lines were drawn as a guide to the eye and correspond to a quadratic dependence of the current on the voltage (Mott-Gurney equation). (a) Au top electrode, measured with the two-point probe configuration. (b) Au top electrode, measured with the four-point probe configuration. (c) MoO_3/Ag top electrode, measured with the four-point probe configuration. Inset: plot of the thickness dependency of the current density at respectively 5 V (a), 1 V (b), and 1 V (c).

However, as shown in Fig. 2(a) for devices using this structure, the voltage dependence of the observed current densities (hole injection through ITO/PEDOT:PSS) deviates from that predicted for a SCLC at high applied voltages where the slope of the double logarithmic current density versus voltage (*J-V*) plots is mainly between 1 and 2. On the other hand at lower voltages, contrary to the expected transition from a quadratic to a linear dependence of the current density on the applied voltage, we observe a slope of the *J-V* plots much larger than 2 for three of the four samples. As the apparent saturation of the current density at high voltages could be due to the series resistance of ITO we also recorded *J-V* plots using a four point configuration as shown in Fig. 2(b) (hole injection through ITO/PEDOT:PSS). Although less outspoken the plots still show a

deviation from a typical SCLC behavior at high applied voltages. Furthermore, even in the voltage range where the slopes of the *J-V* plots are compatible with an SCLC, we observe (see insets of Fig. 2 (a) and (b) that at a fixed voltage (5 V and 1 V in respectively Fig. 2(a) and (b)), the current density does not show the expected inverse cube dependence on the sample thickness. A similar behavior has also been observed by Kumar *et. al.*[43] for the *J-V* characteristics of hole-only devices of P3HT and MEH-PPV. They attributed this behavior to a combination of trap filling and a finite rate of charge carrier injection at the contact. In that case, the charge carrier transport is controlled by both the injecting electrode and the bulk properties of the materials (see SI [28]).

In order to obtain an Ohmic contact for hole extraction we replaced the Au top electrode by a MoO_3/Ag electrode. Deposition of a layer of MoO_3 has been a popular anode modification in OSCs due to its efficient hole injecting properties in combination with simple processing.[44] The MoO_3 films are strongly *n*-type and hole injection proceeds via electron extraction from the HOMO level of the hole transport material through the low-lying conduction band of MoO_3.[44,45] When the MoO_3/Ag electrode is used as a top electrode we on the one hand no longer observe the subquadratic dependence in the *J-V* plots at high applied voltages while on the other hand we observe the expected transition from a linear to a quadratic dependence of the current density at low applied voltages. Furthermore, in contrast to the devices with an Au top-electrode (see insets in Fig. 2 (a) and Fig. 2 (b)), the inset in Fig. 2(c) shows, in agreement with the expression for a SCLC (eq. 1), that at a fixed voltage, in the range where the *J-V* plots show a quadratic dependence (e.g. at 1 V), the current density is proportional to the inverse cube of the film thickness. Hence the currents observed for the samples with PEDOT:PSS and MoO_3/Ag electrodes can be considered as space-charge-limited. If both MoO_3 and ITO/PEDOT:PSS would yield an Ohmic contact for hole injection and extraction one would expect, especially in the voltage range where the *J-V* plots show an SCLC behavior, *J-V* plots that are symmetric for forward and reversed bias. When MoO_3/Ag is used as top electrode this is indeed observed, as shown in Fig. 3(a), for neat P3HT and blended films with a loading by PbS QDs exceeding 60%. This suggests that both electrodes have an excellent hole injection and extraction efficiency and are blocking electron injection. However when Au was used as top electrode such symmetric behaviour was not observed.

For electron only devices, ITO/zinc oxide (ZnO) was used as bottom contact and calcium capped with silver was used as top electrode. ZnO and calcium electrodes provide, due to their low work functions, a hole injection barrier while they can be expected to yield an ohmic contact for electron injection.[29] Therefore, it can be expected that charges can only be injected

into the LUMO of the active material and that the current density is determined by the electron mobility. As shown in Fig. 3(b), the *J-V* plots of P3HT:PbS blended films and neat PbS films incorporated in this structure are symmetrical which indicates that both electrodes provide the same efficiency of electron injection in the different films. Note that, for the electron-only devices it was not possible to obtain a reliable *J-V* curve for a film of neat P3HT.

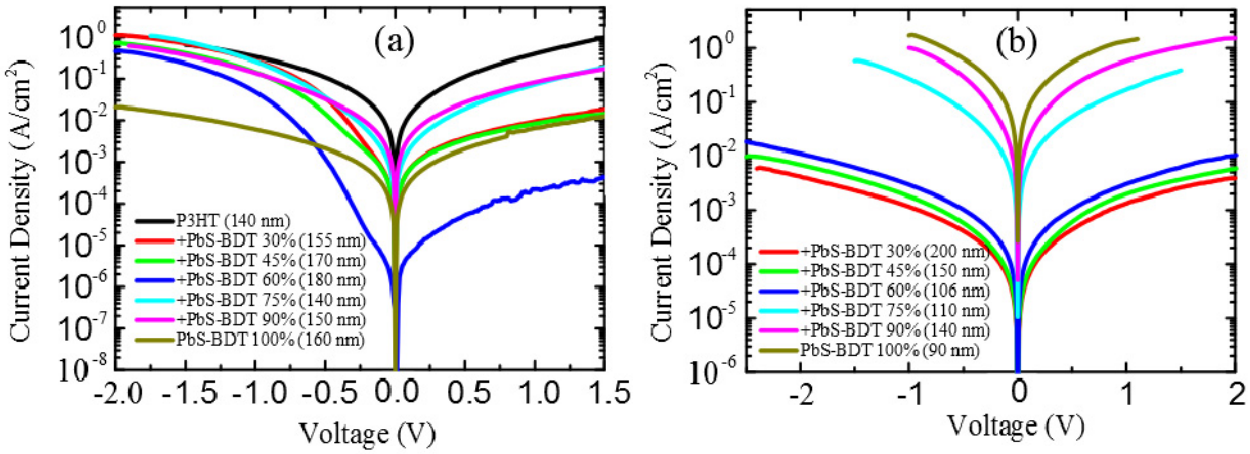

FIG.3. (a) Semi-logarithmic *J-V* curves obtained for (a) hole-only devices (structure: ITO/PEDOT:PSS/active-layer/MoO_3/Ag) and (b) electron-only devices (structure: ITO/ZnO/active-layer/Ca/Ag) of neat P3HT, PbS and P3HT:PbS blended films. The curves were all obtained with the four-point probe configuration. The sign of the voltage corresponds to that of the bottom electrode ((a) ITO/PEDOT:PSS or (b) ITO/ZnO).

To extract the space-charge limited mobility from the hole-only or electron only *J-V* curves, we follow the protocol reported by Blakesley et. al.[46] Several factors such as series resistance and built-in voltage need to be considered and their influence on the charge mobility estimation has to be eliminated or compensated.[46] In this work, the four-point configuration was used to compensate for the external series resistance. The built-in voltage V_{bi} is due to a mismatch between the work-function of the two electrodes and a different structure of two interfaces between the active layer and the electrodes which is observed even when the electrode materials are nominally the same. In our experimental approach V_{bi} is a fit parameter. As the *J-V* characteristics are symmetric versus zero applied potential for almost all the samples, V_{bi} can be put equal to zero, except for the *J-V* plots of hole-only devices of blended P3HT:PbS films where the loading with PbS amounts to 30%, 45%, 60%. As shown by Fig. S5 [28], the *J-V* data acquired in this work were obtained for a sweep from negative voltages to zero volt and then to positive voltages. The sign of the positive voltage corresponds to that applied to the ITO/PEDOT:PSS or ITO/ZnO electrode for hole-only- and electron-only device, respectively. For the samples yielding a symmetric *J-V* curve, the data used

in the fitting procedure correspond to a sweep of the applied voltage from zero volts to positive values. This is because bias stress can affect the shape of the curve when a high voltage is applied for some time (see Fig. S5).[46]

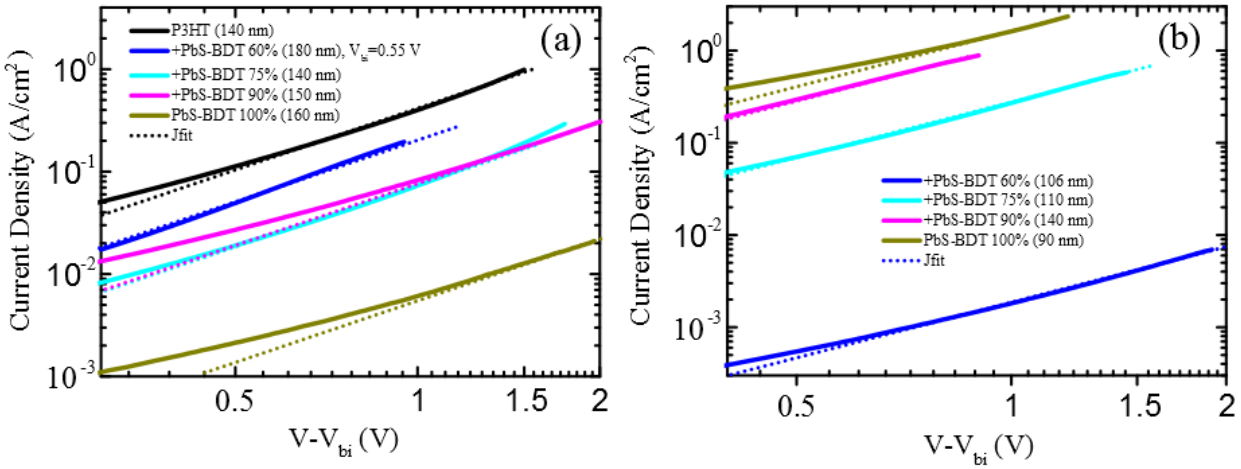

FIG. 4. Exemplary double-logarithmic *J-V* plots of (a) hole-only and (b) electron only devices of P3HT:PbS blends with different PbS loading shown as solid lines. Except for the hole-only device with an active layer of P3HT:PbS 60 %, the *J-V* curves were obtained for the same samples for which linear *J-V* plots are presented in Fig. 3 and correspond to the current densities obtained for positive values of the applied voltage. The dotted lines correspond to fits of the data to Mott-Gurney equation (eq.1). The fitting parameter V_{bi} was put equal to zero except for the hole-only device with an active layer of P3HT:PbS 60 % where the fitting yielded a value of 0.55 V for V_{bi}.

Fig. 4(a)-(b) show the double-logarithmic *J-V* plots obtained for the single carrier devices of pristine P3HT, PbS and P3HT:PbS blended films in the range of data points that was used to calculate the average mobility. The dotted lines in Fig. 4 represent the fits of the experimental data to the Mott Gurney equation (eq. 1) which were used to calculate the average mobility. For the electron-only devices the data could be fitted over a broad range to eq. 1 except for the neat PbS-BDT film where the slope is smaller than predicted by eq. 1 up to an applied voltage of 0.7 V. However for the hole mobility the Mott-Gurney equation is only followed at higher applied voltages, except for the sample with an active layer consisting of a P3HT:PbS 60% blend where it is followed down to less than 0.1 V. Note that, the hole-only current-voltage plot obtained for the P3HT:PbS 60% blend in Fig. 4(a) is shown after correcting the applied voltage by V_{bi}= 0.55 V.

The resulting charge carrier mobilities of the blends are summarized in Fig. 5 and Table S3 [28]. The hole mobility of the pristine P3HT amounted ca. 2.4×10^{-3} $cm^2V^{-1}s^{-1}$ which is higher than the value of 5.6×10^{-4} $cm^2V^{-1}s^{-1}$ determined by Oosterban *et al.*[47] using the SCLC approach. However one should note that the P3HT used by Oosterbaan *et al.* had a lower regioregularity and a higher molecular weight and polydispersity (M_n=23.7 kg/mol, RR=94.5% and PDI=1.8) compared to the RR-P3HT used in the experiments presented in this paper (M_n=13.9 kg/mol, RR>96% and PDI=1.71). The hole mobility

recovered from Sepiolid P200 using the time of flight (TOF) technique amounted to 3×10^{-4} $cm^2V^{-1}s^{-1}$, which is one order lower than the one reported here at a similar field strength ($E \sim 5\times10^4$ Vcm^{-1}).[30] Note that when comparing the hole mobility in Sepiolid P200 to that of P3HT with an RR of 94 % (M_n=34.7 kg/mol and PDI=2.07), using the TOF method, the latter also showed a mobility that was four times smaller.[30]

The difference between the mobilities obtained with the SCLC and the TOF experiments could be due to a different thickness and morphology[43] of the samples used in both experiments as the samples used for the TOF experiments were prepared by drop-casting while those used for the SCLC experiments were prepared by spin coating.[30] It can also not be excluded that the higher carrier densities present in the SCLC experiments lead to partial trap filling and hence a larger mobility.[32,33] We also tried to recover the hole mobility from the current-voltage data of Fig. 2(b), using the non-zero Schottky barrier model[43] (see SI and Table S2 [28]). The hole mobilities and the values of p_0, the carrier density in the active layer at the interface with the electrode (with exception of the 300 nm sample) estimated in this way do not depend significantly upon the sample thickness. Although this gives them some credibility, one should note that the hole mobilities are four to five times smaller than those estimated from the SCLC and two times larger than those obtained by the TOF method. This could possibly be due to a barrier at the extracting electrode (Au) which is not considered in this model and could lead to an underestimation of the mobilities. Hence the mobilities obtained in this way should be considered as a lower limit.

Fitting the *J-V* curves of the sample with a MoO_3 top-electrode to the Mott-Gurney equation, we obtained a hole mobility of 1.5×10^{-3} $cm^2V^{-1}s^{-1}$ for the P3HT:PbS-BDT 60% blended film, which is slightly lower than the hole mobility of pristine P3HT. A further decrease of the hole mobility to (4×10^{-4} and 1.7×10^{-4} $cm^2V^{-1}s^{-1}$), was observed when the loading of the blended films by PbS QDs was increased to 75% and 90% respectively. This modest decrease of the hole mobility is most probably due a decrease of the volume fraction of P3HT in the P3HT:PbS blended films to ca 59 %, 42 % and 19 % respectively (Table S4 [28]). The decrease is of the same order of magnitude as the decrease of the hole mobilities of an "inert" polymer doped with small hole conducting molecules.[48] These results show that in the blended films the holes are transported by P3HT and not by the PbS QDs. The addition of the PbS QDs does not lead to significant trapping of the holes in deep traps. In spite of the observed decrease the hole mobility remains quite large in the blended films which is due to the fact that the blend morphology still provides sufficient percolation paths (*cfr. infra*) for holes even at a 90 % loading by PbS QDs where

the volume fraction of P3HT is still 19 %.[9,10] The hole mobility obtained for a film of neat PbS-BDT QDs amounted to be ca. 1×10^{-5} $cm^2V^{-1}s^{-1}$.

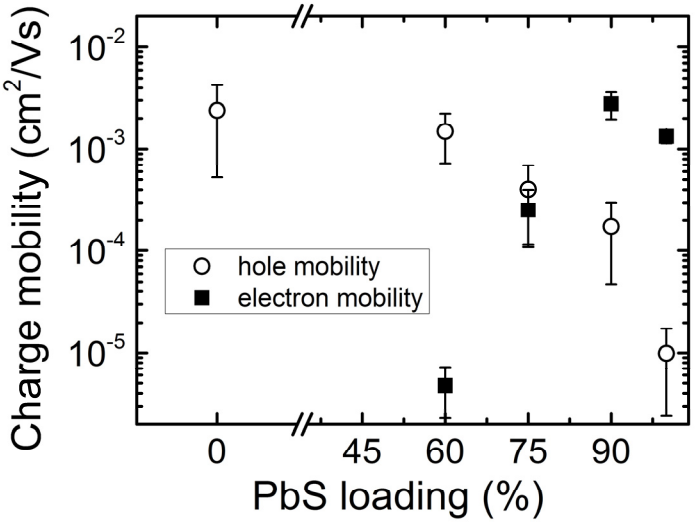

FIG. 5. Hole (■) and electron (○) mobilities of films of neat P3HT, neat PbS QDs and blended P3HT:PbS films with different PbS loading. The mobilities were obtained from fitting the *J-V* curves of the hole-only and electron-only devices with MoO_3/Ag top-electrode to the Mott-Gurney equation (as *e.g.* shown in Fig.4). They should be considered as an average mobility over the voltage range where the Mott-Gurney equation could be applied.

For the electron-only blended devices the slope of the double logarithmic *J-V* curves is close to 2 over a large voltage range which suggests that the electron mobility is nearly independent of the applied field. Only for the film of neat PbS-BDT QDs the slope is clearly smaller when the applied voltage is smaller than 0.4 V. The electron mobility of the film of neat PbS QDs amounted to 1.3×10^{-3} $cm^2V^{-1}s^{-1}$ which is about one order of magnitude higher than the value[38] determined by the time-of-flight technique for a neat film of larger PbS QDs where the original ligand was replaced by ethanedithiol after deposition (diameter ~ 5.9 nm).

In the P3HT:PbS-BDT 60% blended film, containing PbS as electron transport material, an electron mobility of 4.75×10^{-6} $cm^2V^{-1}s^{-1}$ was found. Upon increasing the loading of PbS QDs to 75 % and 90 % the electron mobility is increased by two and three orders of magnitude to respectively 2.5×10^{-4} $cm^2V^{-1}s^{-1}$ and 2.8×10^{-3} $cm^2V^{-1}s^{-1}$. However, we could not obtain usable *J-V* plots for electron-only devices with a neat P3HT film as active layer. Together with the dependence of the electron mobility on the loading by PbS QDs this suggests that the electrons in the blended films are transported by the PbS QDs. This

increase of the electron mobility upon increasing the loading by PbS QDs can be explained in the framework of percolation theory which states that the formation of interconnected paths of small spherical molecules or particles embedded in a three dimensional matrix starts to occur at a volume fraction of 17%.[9,49] For PbS-BDT QDs with a size of ca. 2.4 nm, the percolation threshold in P3HT:PbS blended film can be attained for a loading of about 70% (see Table S4 [28]). While in the P3HT:PbS-BDT 60% blended film the loading is still significantly below the percolation limit the volume fraction of PbS QDs (without the ligands) amounts to respectively 19 % and 26 % in the P3HT:PbS-BDT 75% and P3HT:PbS-BDT 90% blended films (Table S4 [28]). The absence of such strong increase of the mobility at the percolation limit observed by Young [50] for the hole mobility in polystyrene doped by tritolyl amine (TTA) can be due to the much smaller molecular volume of TTA compared to the PbS QDS leading to a much larger concentration and hence a much smaller edge to edge separation at the percolation limit (see FIG S6 (a) supporting information, SI [28]). This leads using the approach of Young [50] at the percolation limit to a mobility that is $2x10^6$ times lower for equidistantly spaced PbS:BDT QDs than for equidistantly spaced TTA molecules (see FIG S6 (b) supporting information, SI [28]). Hence in the neighborhood of the percolation limit hole transport between TTA molecules which are not part of a percolating pathway is still competitive with transport through a percolating pathway. For PbS QDs this is however no longer the case. The possibility to arrive at a non-negligible mobility without clustering or percolation will probably mask the abrupt change of the mobility for the TTA molecules at the percolation limit.

In order to obtain information on the possible loss mechanisms related to electron hole recombination the light intensity dependence of the current-voltage characteristics of solar cells with a P3HT:PbS-BDT bulk heterojunction was investigated. The light intensity was varied over almost two orders of magnitude using a set of neutral density filters. Fig. 6(a) shows the current-voltage characteristics at room temperature of the P3HT:PbS-BDT 90% solar cells for different incident light intensities (7.3, 61.5, 100 and 519 mW/cm^2). An incident light intensity of 100 mW/cm^2 would correspond to the standard 1.5 AM illumination which is broadly used to characterize the performance of photovoltaic devices. The light intensity dependence of the fill-factor is plotted in Fig. 6(b) for solar cells where the active layer is a blended film of P3HT with a loading of 60, 75 and 90% PbS QDs. For all solar cells the fill-factor is decreased significantly at very high intensity (519 mW/cm^2). On the other hand, up to 100 mW/cm^2, the fill factor appears to be less dependent on the light intensity, especially for the solar cells with a 75 and 90 % loading of PbS QDs. This suggests that while up to 100 mW/cm^2 monomolecular processes (first order kinetics) such as geminate or trap-assisted recombination are the major recombination mechanisms, non-geminate recombination starts to dominate at the highest intensity used due to the very high density of generated charge

carriers. In this framework the higher efficiency for charge carrier generation in a blended film with a loading of 90% PbS QDs can also explain why the decease of FF already sets in at lower values of the incident light for a solar cell using this material as active layer. In addition, a large difference in electron- and hole mobility, could also lead to the build-up of a space-charge and a consequent drop of the fill factor at high incident light intensities (*cfr. infra*).

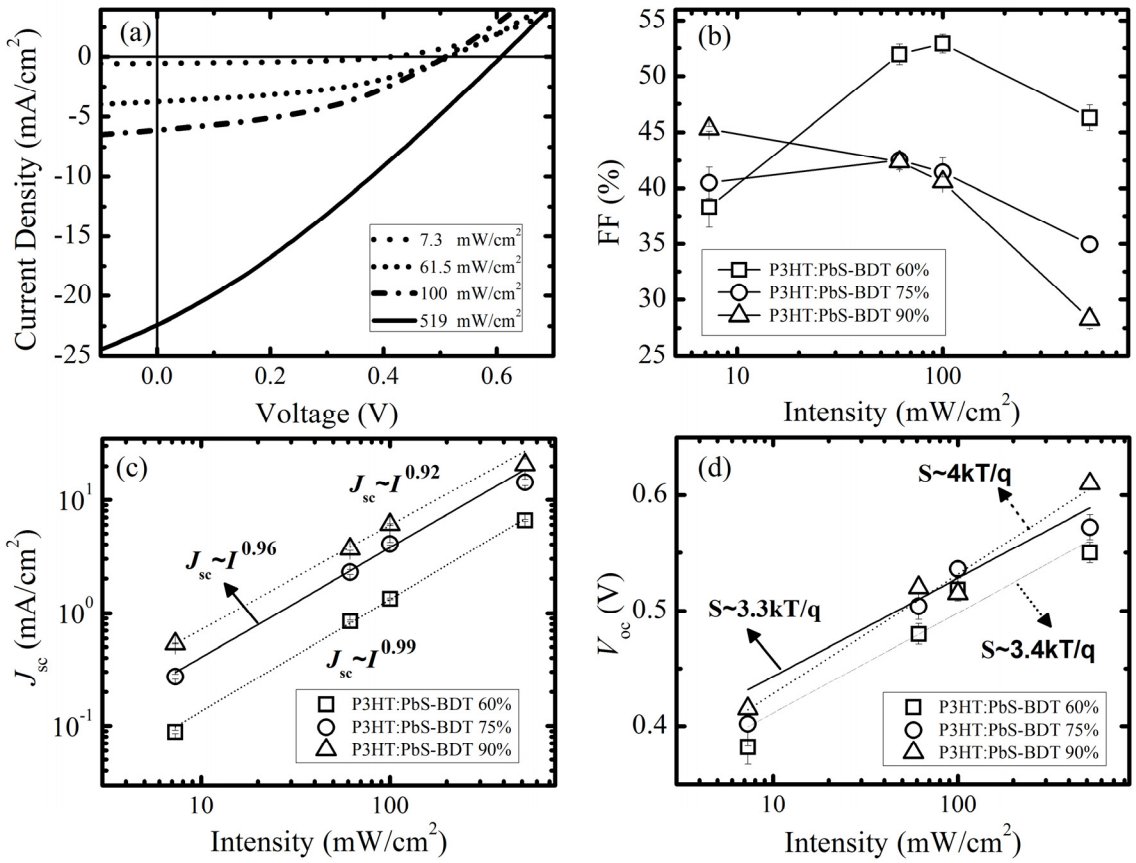

FIG. 6. (a) *J-V* characteristics of (a) a photovoltaic device with an active layer consisting of a blended film of P3HT:PbS-BDT 90% at different incident light intensities. The light intensity dependence of (b) the fill-factor, (c) the short-circuit photocurrent and (d) the open-circuit voltage of photovoltaic devices with as active layer a blended film of P3HT:PbS-BDT (60, 75 and 90% PbS loading).

Fig. 6(c) shows the experimental data of the excitation intensity dependence of the short circuit current density (J_{SC}) which could be fitted from 7.3 to 519 mW/cm^2 to $J_{SC} \sim I^{\alpha}$. Several interpretations have been given to the exponent α, with $\alpha \equiv 1$ indicating that all the carriers, escaping geminate recombination, are swept out prior to recombination.[11] A value of α less than 1 could result from non-geminate recombination or space charge effects.[11,23] The recovered values of α decrease slightly from 0.99±0.03 to 0.92±0.01 upon increasing the concentration of PbS QDs from 60% to 90% , which suggests that although

space-charge effects or non-geminate recombination become more important at 75% and 90% loading by PbS QDs their influence on J_{SC} remains limited. The higher efficiency of charge carrier generation upon increasing the loading by PbS QDs[10] will lead for the same incident light intensity to a larger concentration of charge carriers and hence faster non-geminate recombination. To what extent this will also lead to a larger space charge is less clear. Koster *et al*.[51] reported that the occurrence of space-charge becomes significant when the difference between the mobility of electrons and holes is larger than 2-3 orders of magnitudes. However, while for the solar cells with a blended film of P3HT:PbS-BDT 60% as active layer the electron and hole mobilities differ by nearly two orders of magnitude (see Fig. 5), a value 0.99±0.03 was recovered for α. This implies that in the 60 % blend J_{SC} is not influenced by a potential space charge. Hence this effect is *a fortiori* excluded in the solar cells with a higher loading of PbS-BDT QDs as upon increasing the loading by PbS-BDT QDs the ratio of electron and hole mobility gets closer to one. In addition, as shown in Fig. 6(c), the smaller values of α recovered for the P3HT:PbS-BDT 75 and 90% blended films are to a large extent due to the data-point at the highest light intensity. These results indicate that, in agreement to what was concluded from the light intensity dependence of the fill factor, non-geminate recombination should be taken into account particularly at high light intensity. The comparison between the light intensity dependence of the FF and the J_{SC} shown in Fig. 6(b) and 6(c) also implies that the FF is more sensitive to non-geminate recombination than the J_{SC}. Note that we also reported recently that for solar cells with BDT treated active layers, the increase of PbS the loading systematically decreases the shunt resistance.[9] Finite values of the shunt resistance reflect the presence of current leakage paths through the solar cells which can be attributed to cracks formed after the BDT treatment.[9,10] The shunt resistance and hence the V_{OC} and the FF can be increased by the insertion of a thin layer of neat P3HT below the active layer [9] or of a thin layer of PbS QDs on top of the active layer [10] of the solar cell. The finite values of the shunt resistance can also explain the lower FF of P3HT:PbS-BDT solar cells at higher loading of PbS QDs. [9,52]

Due to the absence of current extraction, which means that all photogenerated charge carriers must disappear by recombination, the properties of the solar cells at open-circuit conditions are strongly dependent on the recombination processes. Fig. 6(d) shows the increase in open-circuit voltage with increasing light intensity for the three devices with a loading of 60 %, 75 % and 90 % of PbS QDs. The increase of the V_{OC} with intensity is the largest for the 90% QD device which suggests the presence of a higher concentration of traps in the device. If Langevin (non-geminate) recombination of free carriers were the only loss mechanism, V_{OC} would be given by[53]

$$V_{OC} = \frac{E_{gap}}{q} - \frac{kT}{q} \ln\left[\frac{(1-P)\gamma N_C N_V}{PG}\right] \quad (4)$$

where E_{gap} is the energy difference between the HOMO of the electron donor (P3HT) and the LUMO of the electron acceptor (PbS), q is electronic charge, k is the Boltzmann constant, T is the temperature, P is the probability of exciton dissociation (including the escape from geminate recombination), γ is the second order recombination rate constant, N_C and N_V are respectively the density of states (DOS) in the conduction of the PbS QDs and the valence band of P3HT, and G is the exciton generation rate. According to this equation which relates V_{OC} to the light intensity; the slope (S) of a plot of V_{OC} versus the logarithm of light intensity should equal to kT/q. However, for devices with 60, 75 and 90% loading by PbS QDs, the experimental data showed a steeper dependence of V_{OC} on the light intensity with S=3.4, 3.3, and 4 times kT/q, respectively. This suggests that recombination at open-circuit condition is dominated by carrier trapping and recombination through traps rather than by non-geminate Langevin recombination. It has been reported that the slope S increases with the strength of the trap-assisted (Shockley-Read-Hall) recombination over Langevin recombination.[17,20,54,55] Nalwa *et al.*[17] showed that in the P3HT:PCBM system the recombination mechanism depends strongly on the processing conditions. For fast-grown devices, in contrast to the slow-grown devices, the trap-assisted recombination dominates over non-geminate Langevin recombination.[17] Mandoc *et al.*[54] showed that deliberately introduction of 7,7,8,8-tetracyanoquinodimethane (TCNQ) electron traps in blends of MDMO-PPV:PCBM strongly modifies the open circuit voltage and its dependence on light intensity (e.g. the slope S changes from 1.05 (kT/q) to 3.04 (kT/q), respectively). Recently, it has been reported also that trap-assisted recombination is responsible for the loss of photogenerated charge carriers in P3HT:CdSe hybrid solar cells.[20] Note that Giansante *et al.*[56] showed that through tailoring the surface chemistry of the QDs in order to control non-covalent and electronic interactions between organic and inorganic components, relatively low trap densities in P3HT:PbS solar cells can be obtained (e.g. show by the slope S equal to kT/q).

IV. CONCLUSIONS

We have investigated solar cells where the active layer consists of blends of P3HT, acting as electron donor and PbS QDs, acting as electron acceptor material. By fabricating single carrier devices, the hole and electron mobilities within the blends were estimated. While the electron mobility in the P3HT:PbS-BDT 60% was found to be very low (4.75×10^{-6} $cm^2V^{-1}s^{-1}$), its significantly increases up to almost three orders of magnitudes upon increasing the PbS loading to 90%. The increase

can be explained by a change in the volume fraction of the PbS QDs which allows one to get beyond the percolation limit. On the other hand, the hole mobility only slightly decreases upon increasing the PbS loading from 60% to 75 and 90% which is due to a decrease of volume fraction of PbS. A similar decrease was also found for blends of organic hole transport materials and inert polymers[48] and for time of flight studies of blended films of P3HT and PbS QDs deposited by drop casting.[30]

Furthermore, the light intensity dependence of the current-voltage characteristics provided insight into the underlying loss mechanisms. The FF was significantly reduced at high light intensity (519 mW/cm^2), which indicates that at this intensity the non-geminate recombination dominates. We also showed that the photocurrent is limited due to the shunt resistance (which in a mechanistic approach is translated in electron hole recombination) rather than by space-charge effects. The light intensity dependence of the open-circuit voltage measurements suggests that recombination at open-circuit condition is dominated by trap-assisted recombination rather than by non-geminate recombination.

ACKNOWLEDGMENTS

This work was supported by the Imec Leuven by a PhD grant to Y.F. and by the EU through FP7 People Herodot (grant 214954). The authors would like to thank Rany Miranti of University of Oldenburg for assistance with sample morphology characterization. We are indebted to the research council of KULeuven through GOA 2006/2, 2011/3 and to Belspo through IAP VI/27 en IAP VII/05.

REFERENCES

[1] K.S. Jeong, J. Tang, H. Liu, J. Kim, A.W. Schaefer, K. Kemp, L. Levina, X. Wang, S. Hoogland, R. Debnath, L. Brzozowski, E.H. Sargent, and J.B. Asbury, ACS Nano **6**, 89 (2012).

[2] H. Nagaoka, A.E. Colbert, E. Strein, E. Janke, M. Salvador, C.W. Schlenker, and D.S. Ginger, J. Phys. Chem. C **118**, 5710 (2014).

[3] M. Aerts, T. Bielewicz, C. Klinke, F.C. Grozema, A.J. Houtepen, J.M. Schins, and L.D.A. Siebbeles, Nat. Commun. **5**, 3789 (2014).

[4] A.J. Nozik, Nano Lett. **10**, 2735 (2010).

[5] R.J. Ellingson, M.C. Beard, J.C. Johnson, P. Yu, O.I. Micic, A.J. Nozik, A. Shabaev, and A.L. Efros, Nano Lett. **5**, 865 (2005).

[6] C. Piliego, H. von Seggern, M. Manca, R. Kroon, M. Yarema, K. Szendrei, M.R. Andersson, and M.A. Loi, J. Mater. Chem. **22**, 24411 (2012).

[7] J. Seo, M.J. Cho, D. Lee, A.N. Cartwright, and P.N. Prasad, Adv. Mater. **23**, 3984 (2011).

[8] J. Yuan, A. Gallagher, Z. Liu, Y. Sun, and W. Ma, J. Mater. Chem. A **3**, 2572 (2015) (DOI: 10.1039/C4TA03995E).

[9] Y. Firdaus, E. Vandenplas, Y. Justo, R. Gehlhaar, D. Cheyns, Z. Hens, and M. Van der Auweraer, J. Appl. Phys. **116**, 094305 (2014).

[10] Y. Firdaus, R. Miranti, E. Fron, A. Khetubol, H. Borchert, J. Parisi, and M. Van der Auweraer, *Charge Separation Dynamics in P3HT:PbS Hybrid Solar Cells*, J. Appl. Phys., under revision by the authors (2015).

[11] S.R. Cowan, A. Roy, and A.J. Heeger, Phys. Rev. B **82**, 245207 (2010).

[12] A. Liu, S. Zhao, S.-B. Rim, J. Wu, M. Könemann, P. Erk, and P. Peumans, Adv. Mater. **20**, 1065 (2008).

[13] R.A. Street, S. Cowan, and A.J. Heeger, Phys. Rev. B **82**, 121301 (2010).

[14] L.J.A. Koster, M. Kemerink, M.M. Wienk, K. Maturová, and R.A.J. Janssen, Adv. Mater. **23**, 1670 (2011).

[15] R. Mauer, I.A. Howard, and F. Laquai, J. Phys. Chem. Lett. **2**, 1736 (2011).

[16] C. Shuttle, B. O'Regan, a. Ballantyne, J. Nelson, D. Bradley, and J. Durrant, Phys. Rev. B **78**, 113201 (2008).

[17] K.S. Nalwa, H.K. Kodali, B. Ganapathysubramanian, and S. Chaudhary, Appl. Phys. Lett. **99**, 263301 (2011).

[18] M.M. Mandoc, W. Veurman, L.J.A. Koster, M.M. Koetse, J. Sweelssen, B. de Boer, and P.W.M. Blom, J. Appl. Phys. **101**, 104512 (2007).

[19] R.A. Street, M. Schoendorf, A. Roy, and J.H. Lee, Phys. Rev. B **81**, 205307 (2010).

[20] F. Gao, Z. Li, J. Wang, A. Rao, I.A. Howard, A. Abrusci, S. Massip, C.R. McNeill, and N.C. Greenham, ACS Nano **8**, 3213 (2014).

[21] D.M. Balazs, M.I. Nugraha, S.Z. Bisri, M. Sytnyk, W. Heiss, and M.A. Loi, Appl. Phys. Lett. **104**, 112104 (2014).

[22] B. Qi and J. Wang, Phys. Chem. Chem. Phys. **15**, 8972 (2013).

[23] V. Mihailetchi, J. Wildeman, and P. Blom, Phys. Rev. Lett. **94**, 126602 (2005).

[24] T. Kirchartz, T. Agostinelli, M. Campoy-quiles, W. Gong, and J. Nelson, J. Phys. Chem. Lett. **3**, 3470 (2012).

[25] W.E.I. Sha, X. Li, and W.C.H. Choy, Sci. Rep. **4**, 6236 (2014).

[26] A. Baumann, J. Lorrmann, C. Deibel, and V. Dyakonov, Appl. Phys. Lett. **93**, 252104 (2008).

[27] R.C. Chiechi, R.W.A. Havenith, J.C. Hummelen, L.J.A. Koster, and M.A. Loi, Mater. Today **16**, 281 (2013).

[28] See supplementary material as [URL will be inserted by AIP] for the configurations of the measurements of the J-V characteristics, the estimation of thechare carrier densities in hybrid solar cells in operating conditions, during SCLC experiments and during time of flight experiments, the morphology of P3HT:PbS blend films, the estimation of the dielectric constant, a model for J-V plots taking into account trap-filling and injection over a non-zero Schottky barrier, the calculation of the charge carrier mobilities, the calculation of the weight and volume fractions of PbS and P3HT from the "loading" bij PbS QDs and the estimation of the concentration dependence of the charge carrier mobilties.. to be resubmitted, J. Polym.Sci. B: Physics.

[29] M.-A. Muth, W. Mitchell, S. Tierney, T.A. Lada, X. Xue, H. Richter, M. Carrasco-Orozco, and M. Thelakkat, Nanotechnology **24**, 484001 (2013).

[30] Y. Firdaus, S. Kudret, A. Khetubol, W. Maes, L. Lutsen, B. Li, W. Frederickx, S. Flamée, W. Vanderlinden, Z. Hens, S. De Feyter, D. Vanderzande, and M. Van der Auweraer, Optical properties, film morphology and hole transport of Poly(3-hexylthiophene) (P3HT) and P3HT/PbS blends, to be submitted. (2015).

[31] C. Tanase, E.J. Meijer, P.W.M. Blom, and D.M. de Leeuw, Phys. Rev. Lett. **91**, 216601 (2003).

[32] C. Tanase, P. Blom, and D. de Leeuw, Phys. Rev. B **70**, 193202 (2004).

[33] M.A. Parshin, J. Ollevier, M. Van der Auweraer, M.M. de Kok, H.T. Nicolai, A.J. Hof, and P.W.M. Blom, J. Appl. Phys. **103**, 113711 (2008).

[34] Y. Shen, A.R. Hosseini, M.H. Wong, and G.G. Malliaras, Chemphyschem **5**, 16 (2004).

[35] C.H. Kim, K. Kisiel, J. Jung, J. Ulanski, D. Tondelier, B. Geffroy, Y. Bonnassieux, and G. Horowitz, Synth. Met. **162**, 460 (2012).

[36] S. Ren, L.-Y. Chang, S.-K. Lim, J. Zhao, M. Smith, N. Zhao, V. Bulović, M. Bawendi, and S. Gradecak, Nano Lett. **11**, 3998 (2011).

[37] J.W. Jung and W.H. Jo, Adv. Funct. Mater. **20**, 2355 (2010).

[38] J. Tang, L. Brzozowski, D.A.R. Barkhouse, X. Wang, R. Debnath, R. Wolowiec, E. Palmiano, L. Levina, A.G. Pattantyus-abraham, D. Jamakosmanovic, and E.H. Sargent, ACS Nano **4**, 869 (2010).

[39] F.F. De Sousa, S.G.C. Moreira, S.J. dos Santos da Silva, J. Del Nero, and P. Alcantara, J. Bionanoscience **3**, 139 (2009) (DOI: org/10.1166/jbns.2009.1013).

[40] D.R. Lide, *CRC Handbook of Chemistry and Physics, Internet Version*, 85th ed. (CRC Press, Boca Raton, Florida, 2005).

[41] P.W.M. Blom, M.J.M. De Jong, and M.G. Van Munster, Phys. Rev. B **55**, 656 (1997).

[42] D. Chirvase, Z. Chiguvare, M. Knipper, J. Parisi, V. Dyakonov, and J.C. Hummelen, J. Appl. Phys. **93**, 3376 (2003).

[43] P. Kumar, S.C. Jain, V. Kumar, S. Chand, and R.P. Tandon, Eur. Phys. J. E. Soft Matter **28**, 361 (2009).

[44] D. Cheyns, B. Kam, K. Vasseur, P. Heremans, and B.P. Rand, J. Appl. Phys. **113**, 043109 (2013).

[45] M. Kröger, S. Hamwi, J. Meyer, T. Riedl, W. Kowalsky, and A. Kahn, Appl. Phys. Lett. **95**, 123301 (2009).

[46] J.C. Blakesley, F.A. Castro, W. Kylberg, G.F.A. Dibb, C. Arantes, R. Valaski, M. Cremona, J.S. Kim, and J.-S. Kim, Org. Electron. **15**, 1263 (2014).

[47] W.D. Oosterbaan, J.C. Bolsee, A. Gadisa, V. Vrindts, S. Bertho, J. D'Haen, T.J. Cleij, L. Lutsen, C.R. McNeill, L. Thomsen, J. V Manca, and D. Vanderzande, Adv. Funct. Mater. **20**, 792 (2010).

[48] M. Van der Auweraer, F.C. De Schryver, P.M. Borsenberger, and H. Bässler, Adv. Mater. **6**, 199 (1994).

[49] C.J. Brabec, F. Padinger, N.S. Sariciftci, and J.C. Hummelen, J. Appl. Phys. **85**, 6866 (1999).

[50] R.H. Young, J. Chem. Phys. **103**, 6749 (1995).

[51] L.J.A.. Koster, V.D. Mihailetchi, H. Xie, and P.W.M. Blom, Appl. Phys. Lett. **87**, 203502 (2005).

[52] N. Zhao, T.P. Osedach, L.-Y. Chang, S.M. Geyer, D. Wanger, M.T. Binda, A.C. Arango, M.G. Bawendi, and V. Bulovic, ACS Nano **4**, 3743 (2010).

[53] L.J.A. Koster, V.D. Mihailetchi, R. Ramaker, and P.W.M. Blom, Appl. Phys. Lett. **86**, 123509 (2005).

[54] M.M. Mandoc, F.B. Kooistra, J.C. Hummelen, B. de Boer, and P.W.M. Blom, Appl. Phys. Lett. **91**, 263505 (2007).

[55] M.M. Mandoc, W. Veurman, L.J.A. Koster, B. de Boer, and P.W.M. Blom, Adv. Funct. Mater. **17**, 2167 (2007).

[56] C. Giansante, R. Mastria, G. Lerario, L. Moretti, I. Kriegel, F. Scotognella, G. Lanzani, S. Carallo, M. Esposito, M. Biasiucci, A. Rizzo, and G. Gigli, Adv. Funct. Mater. **25**, 111 (2015).

Supporting information

Charge transport and recombination in P3HT:PbS solar cell

Yuliar Firdaus,[1] Erwin Vandenplas,[2] Adis Khetubol,[1] David Cheyns,[2] Robert Gehlhaar,[2] and Mark Van der Auweraer[1,a)]

[1] *Laboratory of Photochemistry and Spectroscopy, Division of Molecular Imaging and Photonics, Chemistry Department, KULeuven, Celestijnenlaan 200F, B2404, 3001 Leuven, Belgium*

[2] *Imec vzw, Kapeldreef 75, B-3001 Leuven, Belgium*

a) mark.vanderauweraer@chem.kuleuven.be; phone 3216327496; fax 3216327990

1. Two-point and four-point probe configuration

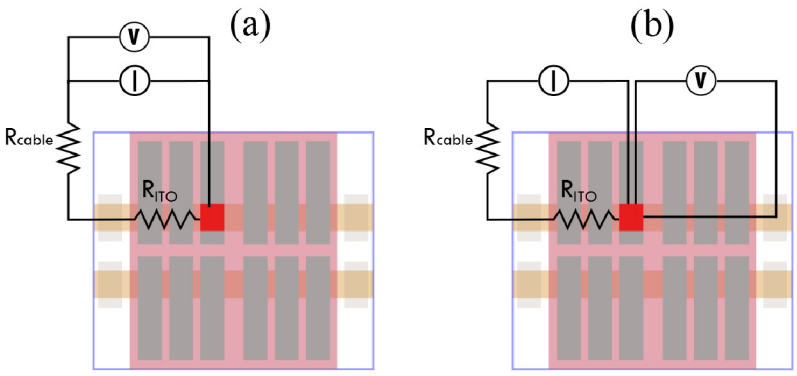

FIG. S1.Scheme of the (a) two-point probe and (b) four-point probe configuration for determination of the *J-V* characteristics of hole-only devices. The *J-V* characteristics of electron-only devices were always measured by four-point probe configuration.

2. Evaluation of the bulk carrier densities in hybrid solar cells under operation, at SCLC conditions in an electron only and hole only device and during TOF experiments

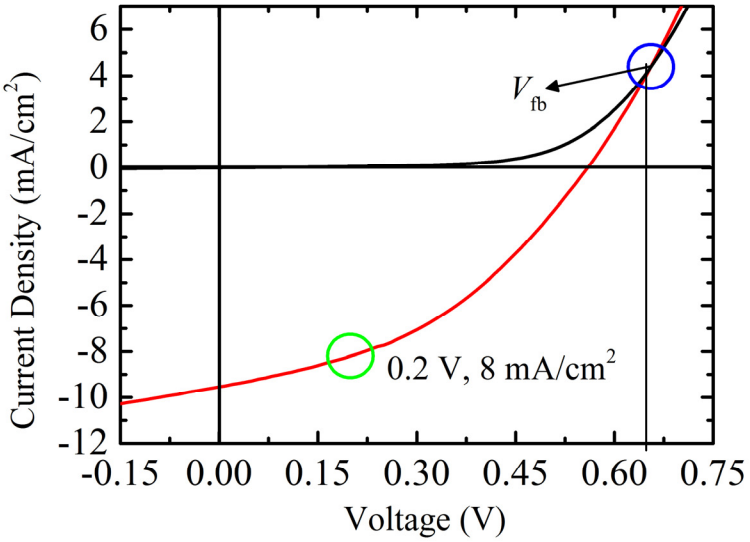

FIG.S2. J-V characteristics of 90 % P3HT:PbS-BDT solar cell device measured in the dark (———) and upon illumination (———, 100 mW/cm^2 AM1.5G).

We first determine the charge carrier density in a hybrid solar cell under operating condition. As an example we choose a P3HT:PbS-BDT 90% solar cell (thickness 100 nm) of which the J-V characteristics are shown in Fig. S2. At a high internal electric field where, we can assume that the current density is drift-dominated (diffusion current can be neglected) the total charge Q (in C) present in the active layer is given by

$$Q(V) = J(V)A\tau \qquad \text{(eq. S1)}$$

Where J is the current density (in A/cm²), A the area of the sample (in cm²) and τ the transit time of the charge carriers (in s). The transit time is given by

$$\tau = \frac{L}{\mu E} \qquad \text{(eq. S2)}$$

Where μ is the charge mobility (in cm²/Vs) and E is the internal electrical field across the sample (in V/cm) and L is the sample thickness (in cm) and amounts to 10^{-5} cm. E is given by

$$E = \frac{V_{fb} - V}{L} \qquad \text{(eq. S3)}$$

where V is the voltage over the solar cell (in V) and V_{fb} is the flat band potential (in V) which corresponds to the voltage where the photocurrent density ($J_{ph} = J_L - J_D$) is zero [1]. V_{fb} is estimated 0.65 V from Fig. S2. J_L and J_D are respectively the current densities under illumination and in the dark. The charge density ρ (in C/cm^3) is given by

$$\rho(V) = \frac{Q(V)}{LA} \qquad \text{(eq. S4)}$$

Combining eq. S1 to S4 the charge density is given by

$$\rho(V) = \frac{J(V)L}{\mu(V_{fb} - V)} \qquad \text{(eq. S5)}$$

This yields for the charge carrier density (in cm^{-3})

$$n(V) = \frac{J(V)L}{\mu e(V_{fb} - V)} \qquad \text{(eq. S6)}$$

Where e is the elementary charge (1.602×10^{-19} C).

Using eq. S6 and at operating conditions (e.g. J = 8 mA/cm^2, V = 0.2 volt), the carrier density is estimated to be around 6.5×10^{15} cm^{-3} for holes and 4.0×10^{14} cm^{-3} for electrons respectively. (for a hole and electron mobility of respectively 1.7×10^{-4} and 2.8×10^{-3} cm^2/Vs).

For the electron and hole only devices the charge carrier density under SCLC conditions can be estimated in a similar way using equation S7.

$$n(V) = \frac{J(V)L}{\mu e(V_{bi} - V)} \qquad \text{(eq. S7)}$$

Where V_{bi} is the built in bias voltage between the electrodes (in V) and V is the applied voltage (in V). Here we find, using eq. S7 with V_{bi} =0 V based on the data in figure 4 for hole only and electron only devices with an active layer of P3HT:PbS-BDT 90% at an applied voltage of 0.5 V respectively 3.3×10^{16} and 1.6×10^{16} charges cm^{-3}.

For the time of flight experiments on neat P3HT (thickness 13.6 m) with identical properties we find at an applied field of 2.9×10^{4} V/cm an injected charge of Q of 1.7×10^{-8} C (fig S10 of the SI of ref 2). As the diameter of the illuminated area equals 0.6 cm in those experiments [2] the illuminated area is 0.28 cm which yields a charge density of 4.4×10^{-5} Ccm^{-3} and a density of mobile charges of 2.8×10^{14} cm^{-3} can be estimated.

3. Morphology of P3HT:PbS blend films

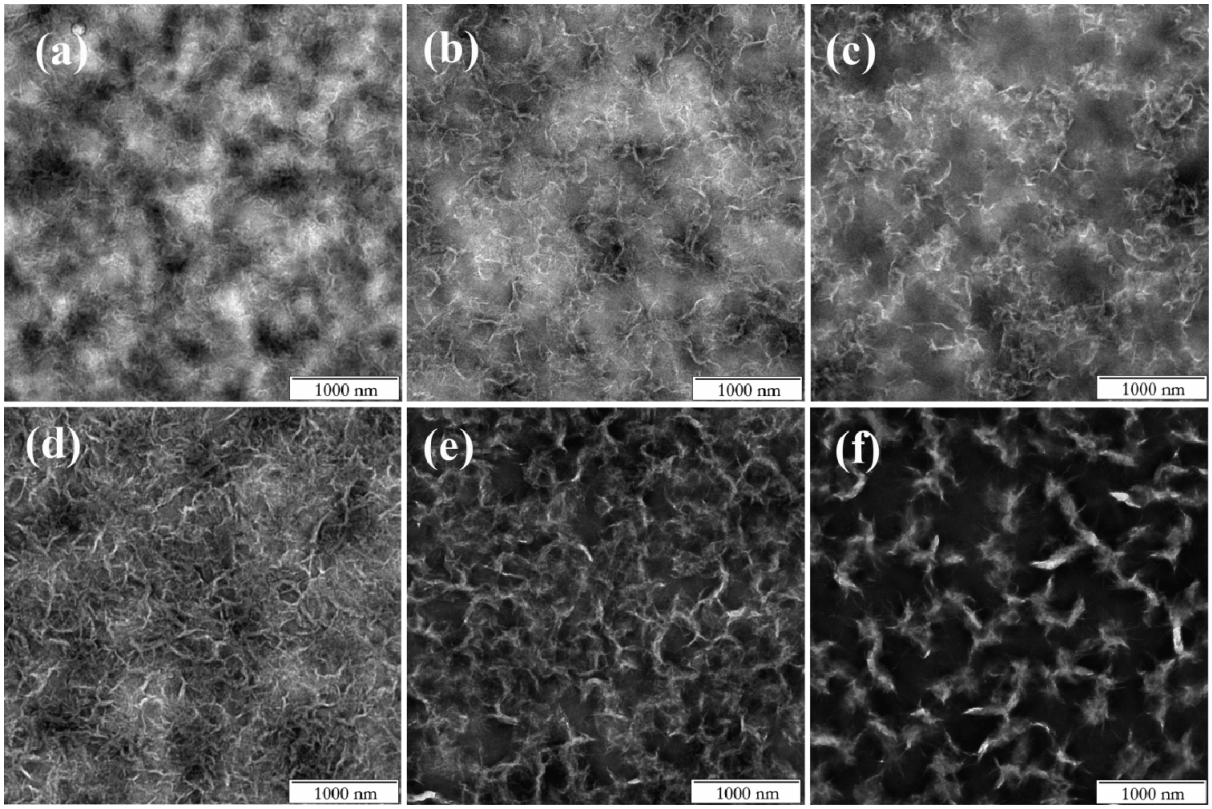

FIG. S3. (a)-(c) TEM images of P3HT:PbS-OLA blend films with different PbS loading (respectively 60%, 75% and 90%) ; (d)-(f) TEM images of P3HT:PbS-BDT blend films with different PbS loading (respectively 60%, 75% and 90%) (scale bar is 1000 nm).

4. Effective dielectric constant

TABLE S1. Effective dielectric constant of P3HT:PbS blended films and neat films of PbS QDs obtained by experiment and by calculations based on the Maxwel-Garnett effective medium theory.

	experiment	calculation		
	$\varepsilon_{eff}(0)$	$\varepsilon_m(0)$	δ	$\varepsilon_{eff}(0)$
P3HT:PbS-OLA 60%	2.55±0.33	3.03	0.089	3.7
P3HT:PbS-OLA 75%	3.62±0.66	2.85	0.111	3.74
P3HT:PbS-OLA 90%	3.5±0.75	2.6	0.133	3.74
neat PbS-OLA	3.85±0.58	2.5	0.147	3.73
P3HT:PbS-BDT 60%	5.94±0.33	3.61	0.133	5.16
P3HT:PbS-BDT 75%	8.82±0.44	3.7	0.188	6.1
P3HT:PbS-BDT 90%	8.93±0.8	3.85	0.26	7.57
neat PbS-BDT	9±0.74	4	0.32	9.15

5. Model for J-V plots taking into account trap-filling model and injection over a non-zero Schottky barrier [3,4]

This model, developed by Jain *et al.*[3], describes the electron and hole transport of single carrier devices (hole- or electron-only devices) in the presence of traps by a combination of the one dimensional Poisson equation the equation describing the drift of the carriers in an applied field. In this model carrier diffusion is neglected.

$$\frac{\mathrm{d}F(x)}{\mathrm{d}x} = \frac{q}{\varepsilon\varepsilon_0}\left(p(x) + p_t(x)\right) \qquad \text{(eq. S8)}$$

$$J = q\mu p(x)F(x) \qquad \text{(eq. S9)}$$

$$V = \int_0^L F(x)\,\mathrm{d}x \qquad \text{(eq. S10)}$$

Where q is the elementary charge, μ the charge carrier mobility, ε and ε_0 are dielectric constant of the material and permittivity of the free space, respectively, $p(x)$ and $p_t(x)$ are respectively the free and trapped charge carrier density, $F(x)$ is the applied field and V is the applied voltage difference over the sample. The model takes into account the contribution of trapped carriers in the Poisson equation through the trapped charge carrier density $p_t(x)$. Assuming an exponential distribution of traps, the trapped charge carrier density is related to the density of free carriers by:

$$p_t(x) = H_b\left(\frac{p(x)}{N_v}\right)^{1/l} \qquad \text{(eq. S11)}$$

Where H_b is the total trap density, N_v the effective density of states in the conduction or valence band and $l=T_c/T$, where T_c is the characteristic temperature of the trap distribution.

The integral of eq. S8 with $p(x)$ and $p_t(x)$ expressed in function of J (through equation S9 and S11) can without any approximation be written as [3,4].

$$\int_0^L \mathrm{d}x = \frac{\varepsilon\varepsilon_0}{q}\int_{F(0)}^{F(L)} \frac{1}{\frac{J}{q\mu F} + H_b\left(\frac{J}{q\mu F N_v}\right)^{1/l}} dF \qquad \text{(eq. S12)}$$

For the case of a non-zero Schottky barrier the injected charge carrier density at the contact is no longer infinitely large but equals a finite number p_0, and hence the boundary condition at x=0 is given by $F=F(0)$, which can be calculated for a given J, μ and p_0 using eq. S9. For a given J, and known thickness L, eq. (S12) was solved numerically to obtain the electric field $F(L)$.[3,4] Next, the electric field $F(x)$ can be determined as a function of x. As $F(x)$ is now known, the voltage V is determined by numerical integration of Eq. (S10). The procedure is repeated for several values of J to obtain the complete J-V characteristic. Some of the J-V characteristics of hole only devices shown in Fig. 2(b) compared with the above simulated results is shown in Fig. S4. The fixed parameters used in the calculation are: ε=3.4, T=300 K, $N_v=1\times10^{19}$ cm^{-3}, while the fitting variables are shown in table S2.

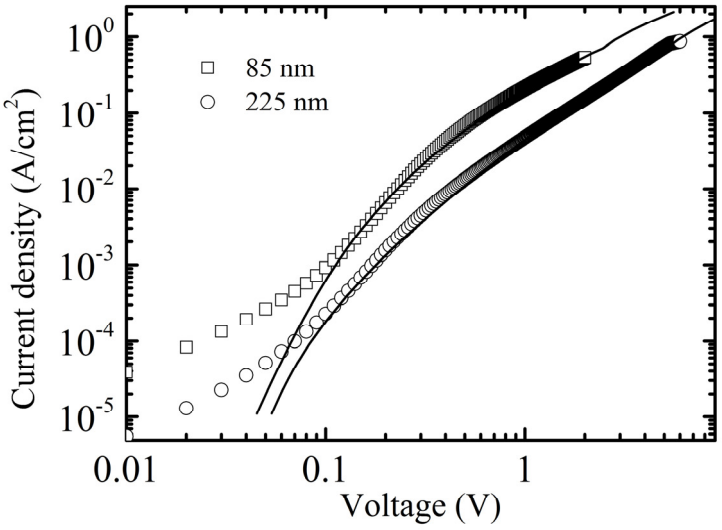

FIG. S4. J-V characteristics of hole only devices with the architecture: ITO/PEDOT:PSS/P3HT/Au measured with a four-point probe configuration (hole injection through the ITO side). The solid line is the J-V-curve simulated by the non-zero Schottky barrier model using eqs. S2 to S6. The values of the fit parameters are shown in Table S2.

TABLE S2. Fit parameters of the *J-V*-curves of hole only devices with architecture ITO/PEDOT:PSS/P3HT/Au and different thicknesses to the non-zero Schottky barrier model.[3]

L (nm)	T_c (K)	μ (cm^2/Vs)	H_b (cm^{-3})	p_0 (cm^{-3})
85	1500	6×10^{-4}	3×10^{16}	3×10^{16}
125	2500	6×10^{-4}	6.5×10^{15}	3.8×10^{16}
225	2500	8×10^{-4}	2×10^{15}	3.5×10^{16}
360	1500	8×10^{-4}	1×10^{12}	3×10^{15}

6. Calculation of the Charge mobilities

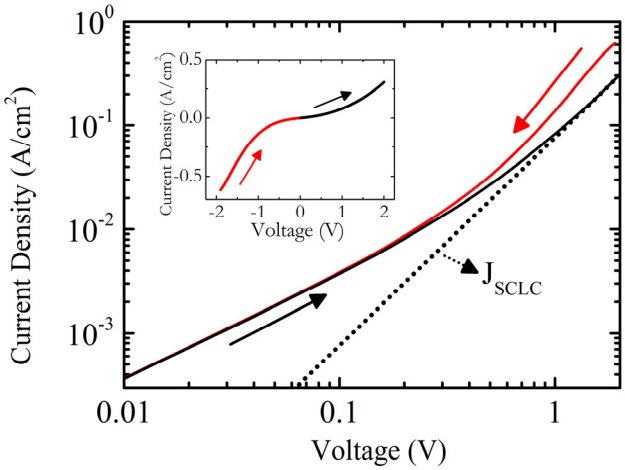

FIG S5. The double-logarithmic current-voltage plot of the hole current in a hole-only device with P3HT:PbS-BDT 90% as active layer is shown with arrows indicating the direction of voltage sweep from respectively -2 to 0 (———) and from 0 to +2 V (———). The data acquired were obtained for a sweep from negative voltages to zero volts then to positive voltages. The sign of the voltage corresponds to that of the ITO/PEDOT:PSS electrode. The dotted line is shown to show the fitting of the current-voltage plot obtained for positive values of to the applied voltage to the Mott-Gurney equation. The inset shows the same data in linear scale.

TABLE S3. Summary of hole and electron mobilities obtained for pristine P3HT, PbS-BDT and P3HT:PbS-BDT blended films. The values were obtained from the *J-V* plots shown in Fig. 4 and the Mott-Gurney equation and represent an average mobility over the voltage range measured.

samples	$\varepsilon_{eff}(0)$	hole mobility (cm^2/Vs)	electron mobility (cm^2/Vs)
P3HT	3.4	$(2.4\pm1.9)\times10^{-3}$	-
+PbS-BDT 60%	5.9	$(1.5\pm0.75)\times10^{-3}$	$(4.75\pm2.5)\times10^{-6}$
+PbS-BDT 75%	8.8	$(4\pm2.9)\times10^{-4}$	$(2.5\pm1.46)\times10^{-4}$
+PbS-BDT 90%	8.9	$(1.7\pm1.3)\times10^{-4}$	$(2.8\pm0.83)\times10^{-3}$
PbS-BDT	9	$(1\pm0.75)\times10^{-5}$	$(1.3\pm0.19)\times10^{-3}$

7. Weight and volume fraction

A detailed discussion on the way how the wt and volume % of P3HT and PbS in the different samples is obtained from the loading is given in the SI of Ref. 5.

TABLE S4. Weight and volume % of PbS QDs and P3HT in P3HT:PbS blends.

Loading in wt% (assuming no ligands are present)	vol% of PbS (for PbS-BDT QDs)	vol% of P3HT (for PbS-BDT QDs)
60	13	59
75	19	42
90	26	19

8. Concentration dependence of the mobility

A major reason for the abrupt rise of the electron mobility in P3HT PbS:BDT blends at the percolation limit compared to the gradual increase of hole mobility observed for polystyrene doped by tritolyl amine (TTA) is due to the much larger volume of a PbS QD (7.23×10^{-27} m^3) versus that of a TTA molecule (5.08×10^{-28} m^3). This leads *e.g.* at a loading of 17 volume % of TTA or PbS QDs (the rest of the volume is occupied by polystyrene or P3HT and the ligands[5]) to 3.35×10^{26} TTA molecules m^{-3} compared to 2.61×10^{25} PbS QDs m^{-3}. As a consequence at the percolation limit the edge to edge distance between two neighboring PbS QDs (including the extra sulfur layer)[6] amounts to 1.73 nm while it amounts to 0.80 nm for two TTA molecules (assuming for both a regular distribution in the matrix). Furthermore we see in figure S6 (a) that upon decreasing the volume fraction of PbS QDs or TTA molecules the edge to edge distance increases much faster for the PbS QDs.

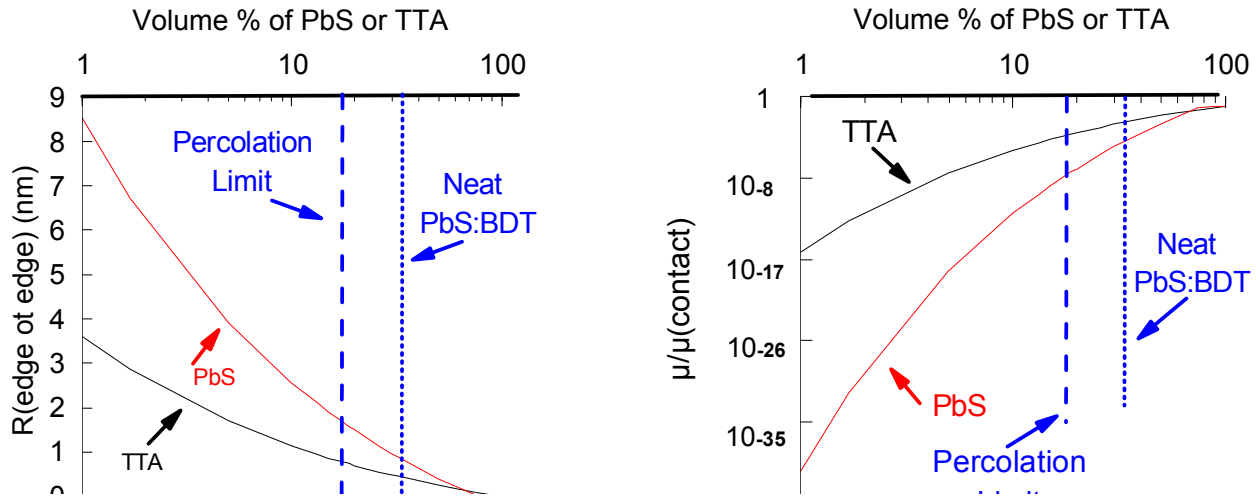

FIG S6. The double-logarithmic plot of (a) the edge to edge distance versus the volume fraction of TTA molecules or PbS QDs; (b) the mobility changes (estimated by eq. S13 and normalized to the mobility expected for neat TTA or neat PbS:BDT QDs versus the volume fraction of TTA molecules or PbS QDs.

We also estimated the dependence of the mobility, μ, on the volume fraction of TTA molecules or PbS QDs (Figure S6 (b)) using following expression of Young[7]

$$\mu \propto R^2 \exp^{-2\alpha R} \qquad \text{(eq.S13)}$$

Where R is the edge to edge distance in Å and α equals 0.56 $Å^{-1}$ according to Young.[7]

Based on eq. S13 the mobility for equidistant transport sites is $2x10^6$ times smaller for PbS QDs than for TTA molecules at the percolation limit. These estimates of the dependence of the mobility on the volume fraction are of course quite rough as 1) especially at low concentration the mobility will be enhanced by the spatial disorder (**Σ**) for both the PbS:BDT QDs and the TTA molecules and 2) we use the value of **α** Young determined for TTA molecules in polystyrene for PbS:BDT QDs in P3HT.

REFERENCES

[1] V. Mihailetchi, L. Koster, J. Hummelen, and P. Blom, Phys. Rev. Lett. **93**, 216601 (2004).

[2] Y. Firdaus, S. Kudret, A. Khetubol, W. Maes, L. Lutsen, B. Li, W. Frederickx, S. Flamée, W. Vanderlinden, Z. Hens, S. De Feyter, D. Vanderzande, and M. Van der Auweraer, Optical properties, film morphology and hole transport of Poly(3-hexylthiophene) (P3HT) and P3HT/PbS blends, to be submitted. (2015).

[3] S.C. Jain, A.K. Kapoor, W. Geens, J. Poortmans, R. Mertens, and M. Willander, J. Appl. Phys. **92**, 3752 (2002).

[4] P. Kumar, S.C. Jain, V. Kumar, S. Chand, and R.P. Tandon, Eur. Phys. J. E. Soft Matter **28**, 361 (2009).

[5] Y. Firdaus, E. Vandenplas, Y. Justo, R. Gehlhaar, D. Cheyns, Z. Hens, and M. Van der Auweraer, J. Appl. Phys. **116**, 094305 (2014).

[6] Y. Firdaus, R. Miranti, E. Fron, A. Khetubol, H. Borchert, J. Parisi, and M. Van der Auweraer, Charge Separation Dynamics in P3HT:PbS Hybrid Solar Cells, submitted J. Appl. Phys. (2014).

[7] R.H. Young, J. Chem. Phys. **103**, 6749 (1995).